Superlattices

DOI: 10.1002/ange.200601233

Superlattice Formation from Polydisperse Ag Nanoparticles by a Vapor-Diffusion Method**

*Yang Yang, Shuman Liu, and Keisaku Kimura**

Plenteous development of synthetic methods affords more and more possibilities to endow nanoparticles with controlled morphology and surface properties that can be manipulated as "artificial atoms". Assembly of these nanoparticles would provide an opportunity to investigate and further tailor their collective physical properties.[1]

Superlattice formation by metal or semiconductor nanoparticles is currently being explored by strategies of bottom-up assembly, which include solvent evaporation of metal nano-organosols on a substrate,[1,2] crystallization of nanoparticles from bulk solution by sedimentation or precipitation,[3] wet deposition by supramolecular interactions between the nanoparticles and a surface,[2d,4] and organization of nanoparticles at oil/water interfaces.[5] In most cases, obtaining superlattice structures strongly depends on highly monodisperse nanoparticles as building blocks. Recently, we reported that hydrophilic metal nanoparticles are excellent components for formation of two- or three-dimensional (2D or 3D) superlattices at the air/water interface by adjusting the concentration of the electrolyte.[6] Herein, we use hydrophilic mercaptosuccinic acid (MSA)-capped Ag nanoparticles as an example and report facile superlattice formation by vapor diffusion of hydrogen chloride (HCl) into their bulk aqueous solution. This new approach can induce the construction of perfect superlattice structure at air/water interfaces under relatively mild conditions and, in particular, high monodispersity of the initial nanoparticle ensemble is not strictly required.

A transmission electron microscopy (TEM) image of the as-prepared MSA-capped Ag nanoparticles (Figure 1a) and their size histogram (Figure 1b) show that they are roughly spherical with an average diameter of 4.8 nm. The full width at half-maximum (fwhm) calculated from the distribution is about 1.4 nm, so the size polydispersity is up to 29%. The

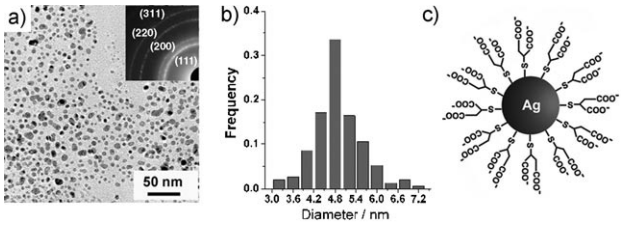

Figure 1. a) TEM image of as-prepared MSA-capped Ag nanoparticles. The inset shows the corresponding SAED pattern. b) Particle size histogram. c) Model of an MSA-capped Ag nanoparticle.

selected-area electron diffraction (SAED) pattern (inset to Figure 1a) shows that the as-prepared Ag nanoparticles consist of a face-centered cubic (fcc) phase (for XRD and FTIR data, see Supporting Information). Figure 1c shows the model of an MSA-capped Ag nanoparticle. On the basis of such a structure, the MSA-capped Ag nanoparticle can be considered to be a macromolecule with good solubility in water and is likely to be modifiable by reaction of the carboxylate groups.[7]

First, we transformed the hydrophilic Ag nanoparticles into organosols by means of the cation surfactant cetyltrimethylammonium bromide ($C_{16}H_{33}(CH_3)_3NBr$, CTAB) through electrostatic interaction. In addition to changing the particle surface from hydrophilic to hydrophobic, the formation of MSA^-–CTA^+ anion–cation pairs effectively neutralizes the charge of the carboxylate groups of MSA. The reduced surface charge is beneficial for the balance between local electrostatic repulsion and dispersion forces required as driving force for self-assembly. However, the high polydispersity of the particles prevented superlattice formation at the air/water interface after solvent evaporation (Supporting Information). Alternatively, we adopted our previous method for growing colloidal crystals of MSA-capped metal nanoparticles from bulk aqueous solution by directly adding a concentrated solution of HCl,[6] which can convert the MSA molecules on the particle surface from the carboxylate to the acid state and thus decrease the repulsive forces among the nanoparticles. However, we failed to obtain any superlattice structures, and the polydispersity of the starting Ag nanoparticles (TEM observations) probably again prevented superlattice formation.

Since MSA-capped nanoparticles can be regarded as artificial macromolecules, the method for the formation of colloidal crystals from bulk solution has certain similarities with practical procedures for macromolecule crystallization. For crystallization of biological macromolecules such as protein/solvent systems, vapor diffusion methods that increase the concentration of precipitating agents or alter physical properties, e.g. the pH value, are currently far more popular than other approaches such as bulk crystallization.[8] The vapor diffusion technique is ideal for screening a large range of conditions and permits considerable flexibility in varying conditions by modification of the precipitant concentration in the reservoir. Hence, we utilized a similar strategy involving gradual diffusion of HCl gas into the concentrated aqueous solution of MSA-capped Ag nanoparticles.

[*] Dr. Y. Yang, Dr. S. Liu, Prof. K. Kimura
Department of Material Science
Graduate School of Material Science
University of Hyogo
3-2-1 Koto, Kamigori-cho, Ako-gun, Hyogo 678-1297 (Japan)
Fax: (+81) 791-580-161
E-mail: kimura@sci.u-hyogo.ac.jp

[**] The Japan Society for the Promotion of Science is gratefully acknowledged for financial support of this work and for a postdoctoral fellowship (P04402). This work was also supported in part by a Grant-in-Aid for Scientific Research (S: 16101003) and Scientific Research in Priority Areas, Molecular Spins (15087210) from MEXT.

Supporting information for this article is available on the WWW under http://www.angewandte.org or from the author.

The crystallization of Ag nanoparticles was carried out in a glass vial (vial A) in which MSA-capped Ag nanoparticle powder (6.0 mg) was dissolved in distilled water (3.0 mL; pH 5.8–6.0); HCl solution (4.0 mL) was placed in another glass vial of the same dimensions (vial B). Then vials A and B were stored in a closed vessel of suitable volume. With 1.0 M HCl solution in vial B, assembled structures visible to the naked eye formed at the air/water interface after about two weeks, while some black precipitate was also observed at the bottom of vial A.

TEM images revealed that most structures formed at the air/water interface consisted of an Ag nanoparticle monolayer over a large area. However, the size of the nanoparticles in the layer was not uniform, so the domain of ordered arrangement was rather small. When the growth period was up to three weeks, 2D superstructures formed at the air/water interface (Figure 2a). A magnified image and the corresponding size histogram are presented in Figure 2b and c, respectively. It can be clearly seen that the MSA-capped Ag nanoparticles organize into a 2D-ordered compact structure. The fast Fourier transform (FFT, inset in Figure 2b) pattern also indicates that the assembly consists of nanoparticle lattices with hexagonal symmetry and long-range order. The average diameter of the particles is about 4.8 nm, and the polydispersity is reduced to 13% in the superlattice. The interparticle gap estimated from Figure 2b is about 1.2 nm, approximately equal to twice the length of the MSA molecule (ca. 0.6 nm), and indicates the absence of chain interdigitation of the MSA layers among adjacent particles. This result agrees well with the mechanism previously proposed for superlattice formation by MSA-capped Au nanoparticles, that is, hydrogen bonds among MSA molecules connect adjacent nanoparticles.[6b,c]

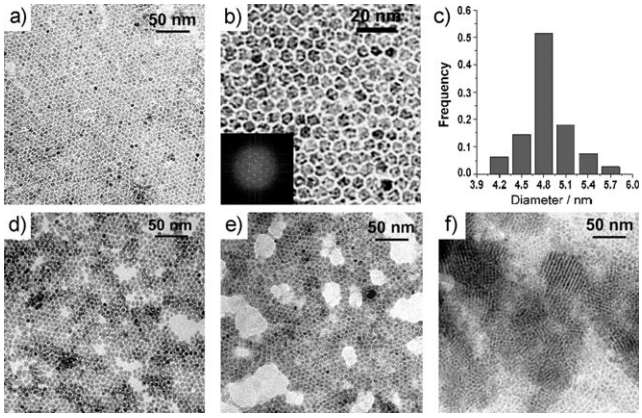

Figure 2. Morphological evolution with aging time for 1.0 M HCl solution in vial B. a) 3, d) 4, e) 5, and f) 7–12 weeks. b) Enlarged image of (a) and corresponding FFT. c) Particle size histogram of (a).

Clearly, the degree of order of the initially formed close-packed 2D structure improves as growth proceeds. Whitesides and Boncheva previously proposed that a sufficient degree of reversibility is required for a self-assembly system to form highly ordered arrays.[9] In our system, the air/water interface not only offers an important alternative scaffold for organization of Ag nanoparticles, but also retains sufficient reversibility to correct errors in the self-assembly process. When the polydisperse hydrophobic Ag nanoparticles assemble into a monolayer at the air/water interface, two important events are likely to happen in this highly dynamic process. First, the particles in the minority whose sizes are different from those of other component particles can be gradually repelled towards the boundary of the superlattice. Second, a particle trapped in a metastable site can be released back into bulk solution owing to its diffusive nature in a suspension (inadequate solvation). Such a particle can possibly reenter the lattice as a building block once the most stable position has been found. These two processes, which act continually during the aging time, will significantly narrow the size distribution in the superstructure, remove lattice defects, and improve the lattice symmetry in the formed superlattice. Simultaneously, the gradual diffusion of HCl into the bulk suspension produces more hydrophobic nanoparticles at a slow rate, which will act as new building blocks and themselves undergo the self-correction process for further growth of the superlattice.

The TEM images shown in Figure 2d and 2e demonstrate the morphological evolution of the superstructures formed at the air/water interface for growth times of four and five weeks. Comparing the contrast of these two images shows that the hexagonal close-packed (hcp) superlattice structure gradually grows from mono- to bi- to multilayer. After growth over a period of seven weeks (the pH in vial A had decreased to 0.4–0.6), many 3D superlattice aggregates were visible (Figure 2f). The close-packed Ag nanoparticles in these superstructures mimic the stacking of atoms in the crystal, and this leads to the appearance of many lattice planes in the colloidal crystal. However, all these 3D superlattices are shapeless and their size is relatively small. Investigation by TEM revealed that this amorphous appearance was hardly changed by further extending superlattice growth to three months. At this time the pH value in vial A was in the range of 0.4–0.6, almost the same as one month earlier, that is, HCl diffusion from vial B to vial A was close to the equilibrium state. Note that the final pH value in vial A is sufficient for superlattice formation according to our previous studies on direct addition of HCl to the bulk solution.

When the initial concentration of HCl in vial B was increased from 1.0 to 3.0 M, assembled structures were found at the air/water interface after only about one week. The shorter time for the appearance of assemblies indicates a faster HCl diffusion from vial B to A. However, unlike the result obtained with 1.0 M HCl solution, most of the formed structures were a mass of particle aggregates, as well as small monolayer domains, according to TEM observations. No large areas of continuous monolayer could be observed. Similarly, the nanoparticle arrangement in these structures was random, and periodic stacking did not take place in the initial stage. Over a growth period of four weeks, the ordering of particle arrangements was partially improved. Figure 3a is a typical image of the structure formed at this stage, from which it can be seen that the particle size in both mono- and multilayers has become uniform, and the particles are inclined to assemble into hcp structures due to the self-

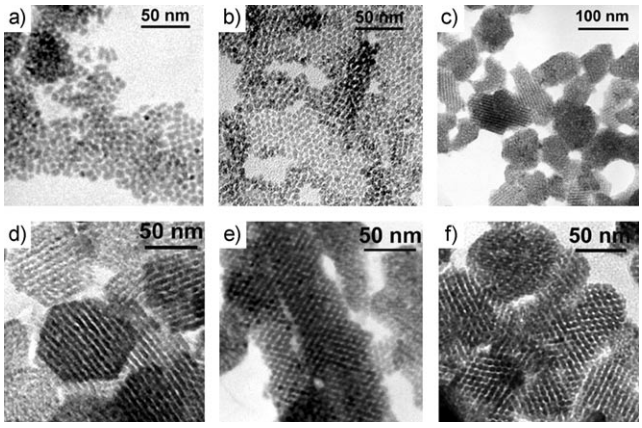

Figure 3. Morphological evolution with aging time for 3.0 M HCl solution in vial B. a) 4, b) 6, and c) 10–12 weeks. d–f) Typical superlattice morphologies during growth for 10–12 weeks.

correction process. After a growth time of 6 weeks, the appearance of ordered mono- and multilayers was observed (Figure 3b). During about 10–12 weeks of growth, a large number of 3D superlattices formed at the air/water interface (Figure 3c). Each 3D superlattice is made up of ordered close-packed nanoparticle, and the superlattices are mostly faceted plate crystals with average size in the range of 50–100 nm. Various shapes of 3D superlattices could be found when different areas of the TEM sample were inspected. Figure 3d–f show three representative morphologies of the 3D superlattices formed under these conditions: hexagonal, clubbed, and round shapes, respectively. In each case, the packing of Ag nanoparticles in the superlattice is very regular.

We further increased the concentration of HCl in vial B to 6.0 M. As expected, the time needed for visible assembly formation at the air/water interface decreased, to 3–4 d. The majority of structures were aggregates composed of randomly arranged nanoparticles. However, the number of aggregates formed in the visual field was smaller than with an initial HCl concentration of 3.0 M. Until six weeks from the beginning, we found some slightly disordered 3D superlattices. A relatively large one is presented in Figure 4a. The observed change in contrast indicates the thickness of overlapping Ag nanoparticle layers is not uniform. The packing of Ag nanoparticles in the thick area is already ordered with the appearance of a regular lattice. However, the particles are not yet well organized in the thin area, which can be assumed to be the origin of further growth of the 3D superlattice. On the basis of self-correction under vapor diffusion, the size of the 3D superlattice became larger and larger with more Ag nanoparticles orderly stacked and overlapping along this direction. Figure 4b and 4c show 3D superlattices for increasing growth time. In every growth stage, the 3D superlattices have the same rhombic shape but with gradually increasing size. After 12 weeks of growth, the cross diameter of the Ag nanoparticle superlattice can attain 1–2 μm. Its thickness was estimated to be 0.2–0.3 μm on the basis of SEM investigations.

Figure 5a and 5b show low- and high-resolution TEM images of a perfectly rhombic 3D superlattice after a growth period of 12 weeks. Compared to the structure shown in Figure 4a, organization of the nanoparticles is much more orderly. The average size of component nanoparticles is still 4.8 nm, but the size polydispersity is reduced from the original 29% to 8% in the superlattice. The projected positions of Ag nanoparticles show a slightly elongated hexagonal structure, which is confirmed by the inset FFT pattern. To discriminate between fcc and hcp structures, further TEM investigation of these superlattices was carried out. Two different arrangements of Ag nanoparticles are found in the superlattice (Figure 5c,d and e,f). Both the observed packing of Ag nanoparticles and the FFT patterns of these arrangements (see insets) are consistent with those expected for the (100) and (110) projections of an fcc superlattice. Especially the strict fourfold symmetry that is apparent in Figure 5d excludes the possibility of an hcp structure.[3b,10] Tilted TEM experiments were performed on the sample grown for 12 weeks. By tilting the 3D superlattice to −15 or +15°, TEM images repeatedly demonstrated that the stacking of Ag nanoparticles in the multilayers always appears to be periodic along various orientations, that is, the 3D superlattice is highly ordered (Supporting Information).

The above investigations show that gradual alteration of pH is particularly beneficial for superlattice formation at the air/water interface no matter which initial concentration of HCl in the reservoir is employed. Increasing the HCl concentration from 1.0, to 3.0, and to 6.0 M increased the

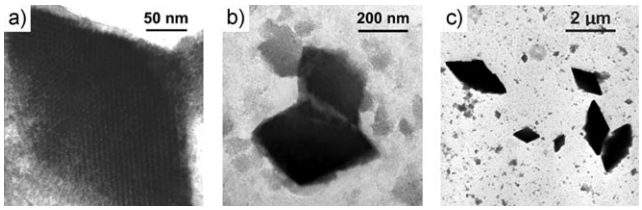

Figure 4. Morphological evolution with aging time for 6.0 M HCl solution in vial B. a) 6, b) 8, and c) 12 weeks.

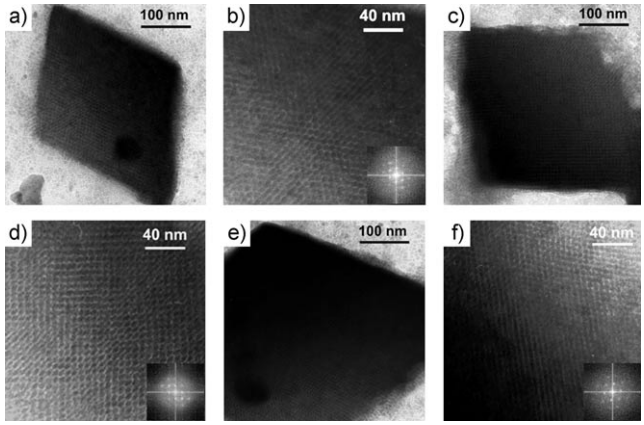

Figure 5. a, c, e) TEM images of three typical 3D rhombic superlattices with 6.0 M HCl solution in vial B during growth of 12 weeks. b, d, f) Enlarged images of (a), (c), and (e), respectively, with corresponding FFT.

rate of diffusion of HCl into the bulk solution of Ag nanoparticles. Accordingly, the appearance of aggregates at the air/water interface became faster and faster. However, at this stage the formed aggregates are random in each case owing to the size polydispersity. By time-dependent self-correction processing, ordered 2D or 3D superlattices began to form at later stages.

Conversely, the time required for superlattice formation was increased by increasing the initial HCl concentration. Since self-correction of the assembly strongly relies on the air/water interface, slower formation of aggregates provides the Ag nanoparticles with sufficient opportunity to self-assemble, restructure, and order themselves into a crystalline lattice at such an interface. Note that, even when 6.0 M HCl solution is used for diffusion, the production of solvates is much milder than with direct addition of concentrated HCl solution. Excessively fast growth will lead to many irregular structures isolated from the air/water interface. This could be the reason why formation of colloidal crystals by direct addition of HCl solution strongly depends on a narrow size distribution of starting nanoparticles and their formation is quite sensitive to the conditions. On the other hand, a lower production rate of building blocks is inclined to form 2D network or 3D crystals of small size. At relatively high diffusion rate, 3D superlattices of large size and characteristic crystal shape become dominant due to full crystal growth, possibly favored by the reduced number of initial nuclei of colloidal crystals. Even if the pH in the hydrosol reaches the same value, the structures formed at the air/water interface under different diffusion conditions are diverse. Thus, the pathway leading to supersaturation and the kinetics of the process may be as important as the final conditions achieved.[8]

In summary, a new vapor diffusion method to build superlattices from polydisperse MSA-capped Ag nanoparticles has been developed. Long-term observations for up to three months demonstrated that superlattice morphology can be controlled by a time- and pH- dependent self-correction process. This represents an economical and general strategy for superlattice creation from water-soluble metal or semiconductor nanoparticles stabilized by molecules bearing carboxylate groups, and is also beneficial for a better understanding of the self-assembly process.

Experimental Section

Preparation of MSA-capped Ag nanoparticles:[7b] With vigorous stirring, freshly prepared aqueous $NaBH_4$ solution (60 mL, 0.2 M) was added through a syringe at a rate of 2.0 mL min^{-1} to water/methanol mixture (250 mL) containing $AgNO_3$ (1.25 mmol) and MSA (97%, 2.5 mmol) at 0 °C. The resulting dark brown, flocculent precipitate was separated and thoroughly washed with 20% water/methanol and pure ethanol in turn, followed by freeze-drying, to yield about 0.25 g of black powder.

Ag nanoparticles were crystallized in a glass vial of 5 cm in height and 1.5 cm in diameter (vial A), in which the as-prepared MSA-capped Ag nanoparticle powder (6.0 mg) was dissolved in distilled water (3.0 mL) to form a dark brown solution. HCl solution (4.0 mL) was placed in another glass vial (vial B). The concentration of HCl solution in vial B was set at 1.0, 3.0, or 6.0 M. Then vials A and B were stored in a closed vessel of suitable volume (50 mL) and left in the dark for three months. The species formed at the air/water interface in vial A were sampled after certain times for morphology observations.

TEM images and corresponding SAED patterns were obtained at 200 kV acceleration voltage. The Ag nanoparticle superstructures formed at the air/water interface were directly transferred to a carbon-coated copper support grid for TEM and SAED experiments. The mean particle size of Ag nanoparticles was estimated by measuring the diameters of at least 200 individual particles. SEM images were taken at 15 kV acceleration voltage. X-ray diffraction (XRD) was performed with $Cu_{K\alpha 1}$ radiation ($\lambda = 1.54056$ Å) at 40 kV and 20 mA.

Received: March 29, 2006
Revised: April 28, 2006
Published online: July 26, 2006

Keywords: nanoparticles · self-assembly · silver · superlattices

[1] a) H. Weller, *Curr. Opin. Colloid Interface Sci.* **1998**, *3*, 194; b) C. P. Collier, T. Vossmeyer, J. R. Heath, *Annu. Rev. Phys. Chem.* **1998**, *49*, 371; c) C. B. Murray, C. R. Kagan, M. G. Bawendi, *Annu. Rev. Mater. Sci.* **2000**, *30*, 545; d) B. O. Dabbousi, C. B. Murray, M. F. Rubner, M. G. Bawendi, *Chem. Mater.* **1994**, *6*, 216; e) P. C. Ohara, J. R. Heath, W. M. Gelbart, *Angew. Chem.* **1997**, *109*, 1120; *Angew. Chem. Int. Ed. Engl.* **1997**, *36*, 1078; f) S. A. Harfenist, Z. L. Wang, R. L. Whetten, I. Vezmar, M. M. Alvarez, *Adv. Mater.* **1997**, *9*, 817; g) M. P. Pileni, *J. Phys. Chem. B* **2001**, *105*, 3358; h) S. Stoeva, K. J. Klabunde, C. M. Sorensen, I. Dragieva, *J. Am. Chem. Soc.* **2002**, *124*, 2305; i) F. X. Redl, K. S. Cho, C. B. Murray, S. O'Brien, *Nature* **2003**, *423*, 968; j) E. V. Shevchenko, D. V. Talapin, N. A. Kotov, S. O'Brien, C. B. Murray, *Nature* **2006**, *439*, 55.

[2] a) A. Taleb, C. Petit, M. P. Pileni, *Chem. Mater.* **1997**, *9*, 950; b) A. L. Rogach, D. V. Talapin, E. V. Shevchenko, A. Kornowski, M. Haase, H. Weller, *Adv. Funct. Mater.* **2002**, *12*, 653; c) S. I. Stoeva, B. L. V. Prasad, S. Uma, P. K. Stoimenov, V. Zaikovski, C. M. Sorensen, K. J. Klabunde, *J. Phys. Chem. B* **2003**, *107*, 7441; d) M.-C. Daniel, D. Astruc, *Chem. Rev.* **2004**, *104*, 293.

[3] a) C. B. Murray, C. R. Kagan, M. G. Bawendi, *Science* **1995**, *270*, 1335; b) D. V. Talapin, E. V. Shevchenko, A. Kornowski, N. Gaponik, M. Haase, A. L. Rogach, H. Weller, *Adv. Mater.* **2001**, *13*, 1868.

[4] a) L. M. Demer, D. S. Ginger, S.-J. Park, Z. Li, S.-W. Chung, C. A. Mirkin, *Science* **2002**, *296*, 1836; b) A. K. Boal, F. Ilhan, J. E. DeRouchey, T. Thurn-Albrecht, V. M. Rotello, *Nature* **2000**, *404*, 476; c) A. Sanyal, T. B. Norsten, O. Uzun, V. M. Rotello, *Langmuir* **2004**, *20*, 5958.

[5] a) Y. Lin, H. Skaff, T. Emrick, A. D. Dinsmore, T. P. Russell, *Science* **2003**, *299*, 226; b) W. H. Binder, *Angew. Chem.* **2005**, *117*, 5300; *Angew. Chem. Int. Ed.* **2005**, *44*, 5172.

[6] a) K. Kimura, S. Sato, H. Yao, *Chem. Lett.* **2001**, 372; b) S. H. Wang, S. Sato, K. Kimura, *Chem. Mater.* **2003**, *15*, 2445; c) S. H. Wang, H. Yao, S. Sato, K. Kimura, *J. Am. Chem. Soc.* **2004**, *126*, 7438.

[7] a) S. H. Chen, K. Kimura, *Langmuir* **1999**, *15*, 1075; b) S. H. Chen, K. Kimura, *Chem. Lett.* **1999**, 1169; c) J. Tominaga, S. Sato, H. Yao, K. Kimura, *Chem. Lett.* **2002**, 950.

[8] A. McPherson, *Crystallization of Biological Macromolecules*, Cold Spring Harbor, Cold Spring Harbor, **1999**.

[9] G. M. Whitesides, M. Boncheva, *Proc. Natl. Acad. Sci. USA* **2002**, *99*, 4769.

[10] a) L. Motte, F. Billoudet, E. Lacaze, J. Douin, M. P. Pileni, *J. Phys. Chem. B* **1997**, *101*, 138; b) Z. L. Wang, *Adv. Mater.* **1998**, *10*, 13.

